

PACS numbers: 74.72.–h; 74.80.Dm
DOI: 10.1070/QE2002v032n12ABEH002350

Interlayer electrodynamics of high-T_c superconductors: an experimental overview

D.N. Basov

***Abstract*. An astonishing feature of underdoped high-T_c superconductors is that the energy scale associated with the formation of superconducting condensate dramatically exceeds the energy gap and appears to be of the interband caliber [1]. This effect can be interpreted in terms of lowering of the electronic kinetic energy at $T < T_c$ and thus points to a mechanism of superconductivity radically departing from the Bardeen – Cooper – Schrieffer (BCS) theory. This nontrivial superconducting state electrodynamics appears to be directly connected to anomalies of cuprates observed in the normal state, including the pseudogap, and to the lack of well-defined quasiparticles.**

Keywords: *high-T_c superconductors, superconducting gap, infrared spectroscopy, pseudogap state.*

Superconductivity at high critical temperature has been so far achieved only in layered copper oxide materials. This class of compounds reveals a remarkable anisotropy of electronic properties. The behaviour of most cuprates when probed with currents or electric field along the CuO_2 planes can be characterised as 'metal-like'. However, these planes appear to be nearly decoupled, at least in the normal state and a variety of properties probed in the interlayer c-axis direction are insulator-like [2]. In many series of cuprates, the transition temperature is enhanced with increasing the number of CuO_2 layers per unit cell [3]. Nevertheless, at least two compounds with only one CuO_2 layer/unit cell such as $Tl_2Ba_2CuO_{6+x}$ (Tl2201) and $HgBa_2CuO_{4+x}$, show the values of T_c above 90 K. At least one model: the interlayer tunneling theory (ILT) makes an explicit connection between nearly insulating c-axis response predetermined by the layered crystal structure and high critical temperature [4, 5]. Generally, the role played by the interlayer coupling in the formation of the high-T_c state has been the focus of attention ever since the discovery of the high-T_c phenomenon.

Infrared and optical spectroscopy is ideally suited to explore the fundamentals of the interlayer transport. Indeed, this experimental technique allows one to directly probe the density of superconducting condensate relevant to Josephson coupling between nearly isolated CuO_2 planes [6]. Spectroscopic experiments also provide valuable information on the superconducting energy gap and the so-called pseudogap state that develops in many cuprates at $T^* > T_c$ [7]. Recent technical advances now permit an examination of the interlayer transport on microscopic samples [8] so that a variety of high-T_c materials can be investigated. The infrared studies of the interlayer electrodynamics enable inference of generic trends and common patterns in complex behaviour of cuprate superconductors. In this article, the author reviews some of the recent experiments aimed at probing the energy scales relevant to the superconducting transition, as well as the issues pertinent to the breakdown of the Fermi liquid description of the interlayer response.

Gross features of the interlayer response of cuprates can be readily recognised in raw reflectance data displayed in Fig. 1 for $La_{2-x}Sr_xCuO_4$ (La214) [9]. Owing to strong anisotropy, the reflection spectra recorded in the normal state with $\boldsymbol{E}$ being parallel to the c axis are 'insulator-like': several pronounced phonon modes are observed at $\omega > 200$ cm^{-1} and a flat, frequency-independent background in the far-IR region where $R(\omega) = 0.5 - 0.6$ [10 – 12]. The spectra only weakly depend on temperature as T decreases from 300 K down to T_c. However, as soon as these samples undergo the superconducting transition, the reflectance immediately changes its character: $R(\omega)$ nearly reaches unity at the lowest frequencies and then abruptly drops down to about 0.2. At higher energies, reflectance slowly

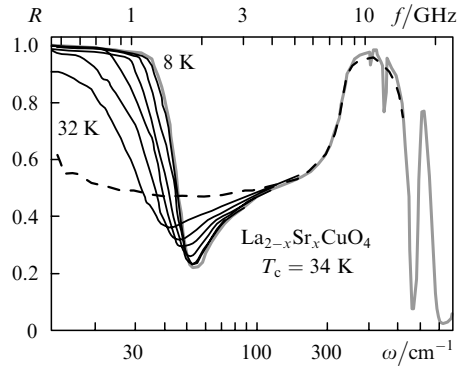

Figure 1. Spectra of the c axis reflectivity for the single $La_{2-x}Sr_xCuO_4$ crystal with $T_c = 34$ K measured at 8 K (gray line), 17 K, 20 K, 22 K, 25 K, 27 K, 32 K (thick solid lines) and 37 K (dashed line) [9]; f is the radiation frequency.

D.N. Basov Department of Physics, University of California, San Diego, La Jolla, CA 92093-0319 USA; e-mail: dbasov@physics.ucsd.edu

Received 25 October 2002
Kvantovaya Elektronika **32** (12) 1080 – 1084 (2002)
Submitted in English

recovers to the magnitude observed in the normal state. This behaviour resembles the plasma resonance that occurs in ordinary metals.

The plasma edge can be viewed as an immediate consequence of the formation of superconducting $\delta(0)$-peak in the real part of the complex conductivity $\sigma(\omega) = \sigma_1(\omega) + i\sigma_2(\omega)$ [10, 13]. Because the plasma edge appears to be associated with the Josephson coupling of CuO_2 layers, this feature is often referred to as the Josephson plasma resonance (JPR). The electronic conductivity both below and above T_c is strongly temperature dependent (Fig. 2). The absolute values of $\sigma_1(\omega)$ obtained from the Kramers–Kronig analysis of the spectra $R(\omega)$ in Fig. 1 are relatively small and do not exceed 15 Ω^{-1} cm^{-1} in the limit of $\omega \to 0$. As carrier concentration is increased upon doping, the absolute values of $\sigma_1(\omega)$ increase as well. Eventually, the Drude-like mode evolves in the interlayer conductivity (see Fig. 5). The strength of the superconducting condensate ρ_s proportional to the area under the $\delta(0)$-peak in the spectrum $\sigma_1(\omega, T \ll T_c)$ is calculated from the suppression of the conductivity below T_c and also increases upon doping.

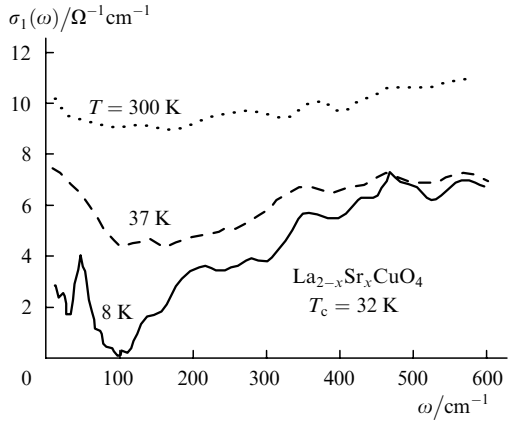

Figure 2. Spectra of the real part of the conductivity obtained from Kramers–Kronig analysis of the reflectance data shown in Fig. 1 Only the electronic background is shown. Phonon peaks have been removed by fitting with Lorentzian oscillators.

It is customary to characterise the condensate strength in a superconductor by the penetration depth $\lambda = (1/\rho_s)^{1/2}$. The interlayer penetration depth λ_c in several families of cuprates reveals a universal scaling dependence on the dc conductivity σ_{dc} ($T = T_c$) (Fig. 3) [9, 14]: the absolute value of λ_c systematically decreases with increasing the normal state conductivity. The scaling is observed primarily in under-doped cuprates (block symbols in Fig. 3). The deviations from the scaling are also systematic and are most prominent in over-doped phases (open symbols in Fig. 3). Such deviations are a direct consequence of a well-established fact that on the over-doped side of the phase diagram, σ_{dc} increases, whereas λ_c is either unchanged or may show a minor increase [12, 15, 16].

A similar scaling pattern between λ_c and σ_{dc} is also observed in other classes of layered superconductors, including organic materials, transition-metal dichalcogenides and Sr_2RuO_4. While the non-cuprate data set is not nearly as dense, the key trend is analogous to the one found for cuprates. The slope of the dependence $\lambda_c(\sigma_{dc})$ is also close for cuprates and non-cuprate materials. The

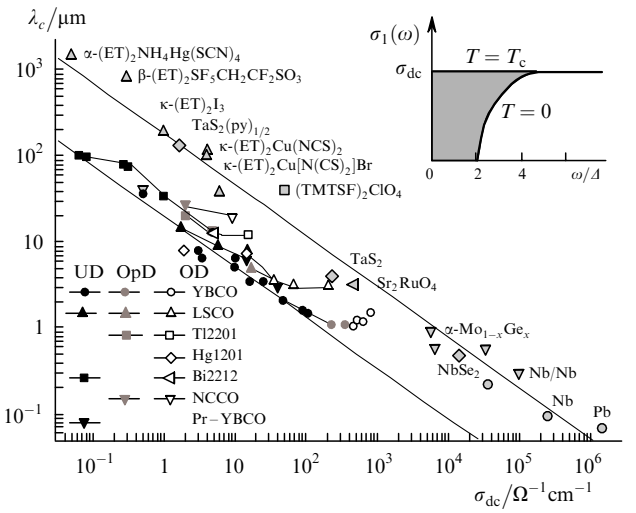

Figure 3. The penetration depth λ_c ($T \to 0$) along the c axis as a function of the dc conductivity σ_{dc} for a variety of layered superconductors [14]. We found two distinct patterns of the $\lambda_c(\sigma_{dc})$ scaling. Cuprate superconductors exhibit much shorter penetration depths than non-cuprate materials with the same $\sigma_{dc}(T_c)$. This result may be interpreted in terms of a dramatic enhancement in the energy scale from which the condensate is collected, as described in the text. See Ref. [14] for the discussion of the raw data points and analysis. Inset: in a conventional dirty superconductor, the spectral weight of the superconducting condensate (given by $1/\lambda^2$) is collected primarily from the energy gap region. The total normal weight is preset by the magnitude of σ_{dc}, whereas the product $2\Delta\sigma_{dc}$ determines the fraction of the weight that condenses.

principal difference is that the universal dependence for cuprates is shifted down by approximately one order of magnitude in λ_c. This shows that the superfluid density is significantly enhanced in under-doped cuprates compared to non-cuprate materials with the same dc conductivity. The superconducting transition temperature T_c has not been found to be relevant to the $\lambda_c(\sigma_{dc})$ scaling. The authors of paper [14] concluded that the two distinct patterns in the plot $\lambda_c(\sigma_{dc})$ could be understood in terms of a dramatic increase in the energy scale, from which the superconducting condensate is accumulated in underdoped cuprates, compared to that in more conventional layered superconductors.

A spectroscopic study of the interlayer electrodynamics enables explicit examination of the energy scales associated with the superconducting transition. This capability is afforded by the sum rule analysis of the conductivity data [17, 4, 5, 1]. For this purpose, it is instructive to introduce the effective spectral weight defined as $N(\omega) = \int_0^{\omega} \sigma_1(\omega')d\omega'$, and then to examine the difference between the above integrals in the normal and superconducting state: $N_n(\omega) - N_s(\omega)$. This difference characterises the process of the condensate formation [1]. In a conventional BCS superconductor, about 70 % – 80 % of the condensate density is accumulated from energies of the order of the energy gap 2Δ, as schematically illustrated in the inset in Fig. 3. The condensation is nearly complete as ω reaches $(5-6)\Delta$. Interestingly, in many cuprates (primarily in underdoped phases), a significant fraction of the superconducting condensate is produced at energies significantly exceeding the energy gap [1]. This effect can be interpreted in terms of lowering of the electronic kinetic energy at $T < T_c$.

Experimental results for several families of materials are summarised in Fig. 4. Here, we plot the ratio $[N_n(10\text{ K}) -$

$N_s(T = T_c)]/\rho_s$ as a function of the dc conductivity across the layers. The integrals in the numerator were calculated up to a cut-off energy of 0.1 eV. The deviation of $[N_n(10\ K) - N_s(T = T_c)]/\rho_s$ from unity quantifies the amount of spectral weight in the δ(0)-peak that originates from anomalously high frequencies ($\omega \gg 2\Delta$) and is therefore related to lowering of the kinetic energy. It appears that the high frequency contribution to the condensate density is most prominent in the materials with low dc conductivity. As σ_{dc} increases, the $[N_n(10\ K) - N_s(T = T_c)]/\rho_s$ ratio increases monotonically up to unity, implying that the sum rule is exhausted with the relatively narrow cut-off of 0.1 eV. This trend is similar in a variety of cuprates, including $YBa_2Cu_3O_x$ (Y123), Tl2201 and La214. At least in Y123 and in La214 systems, the changes in the c-axis component of the kinetic energy are clearly related to the development of the pseudogap state at $T^* > T_c$ and to the 'insulating' behaviour observed in the temperature dependence of the resistivity. The signature of the pseudogap in the *c*-axis response of under-doped high-T_c cuprates is the transfer of the spectral weight from far-infrared to higher energies [18]. This process corresponds to the suppression of $\sigma_1(\omega \to 0)$ (see Fig. 2) and to a characteristic 'semiconducting' temperature dependence of the dc resistivity, which is commonly found in underdoped compounds. With the exception of Tl2201, all materials in Fig. 4, for which $[N_n(10\ K) - N_s(T = T_c)]/\rho_s < 1$ is smaller than unity show the 'semiconducting' resistivity. In the pseudogap state, the charge carriers become more strongly confined to the CuO_2 planes, while the probability of their coherent hopping across the planes is reduced. Therefore, data in Fig. 4 are indicative of the fact that the change in the kinetic energy at $T < T_c$ may be related to a degree of coherence in the interlayer response in the normal state. Note also that the changes in the kinetic energy are of the same order as the magnitude of the *c* axis kinetic energy itself. This interesting regime has to be contrasted with what typically occurs in superconducting metals.

Anomalous features of the interlayer electrodynamics observed in high-T_c materials appear to be related to the character of electromagnetic response probed with the electric field parallel to the CuO_2 planes. In this context,

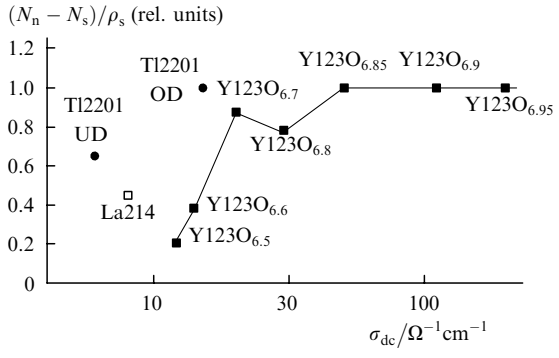

Figure 4. Normalised spectral weight $[N_n(10\ K) - N_s(T = T_c)]/\rho_c$ obtained from the integration of the interlayer conductivity up to the cut-off energy 0.1 eV. The $[N_n(10\ K) - N_s(T = T_c)]/\rho_c$ data for a variety of high-T_c cuprates are plotted as a function of the dc conductivity along the *c* axis at T_c. With the exception of the optimally-doped $Tl_2Ba_2CuO_6$, all samples, in which $[N_n(10\ K) - N_s(T = T_c)]/\rho_c$ is smaller than 1, show 'semiconducting' upturn in the temperature dependence of the dc resistivity.

it is instructive to inquire if the in-plane properties are indicative or not of well-defined quasiparticles in the system. A quantity relevant for this inquiry is the in-plane scattering rate defined as:

$$\frac{1}{\tau_{ab}(\omega)} = \frac{\omega_p^2}{4\pi} \frac{\sigma_1(\omega)}{\sigma_1^2(\omega) + \sigma_2^2(\omega)}. \quad (1)$$

The plasma frequency ω_p in Eqn (1) can be obtained from the integration of the real part of the optical conductivity up to the frequency corresponding to the onset of interband absorption. The bottom panels in Fig. 5 show the *in-plane* scattering rate (inverse lifetime) for high-T_c materials and for a conventional layered superconductor $2H-NbSe_2$, whereas the top panel displays corresponding data for the *interplane* conductivity. An important feature of the data presented in Fig. 5 is that, as doping is increased from underdoped $YBa_2Cu_3O_{6.6}$ to optimally doped $YBa_2Cu_3O_{6.9}$, the absolute values of $1/\tau_{ab}(\omega)$ decrease. A similar trend is observed in other cuprates [19, 23–25]. The shaded regions in Fig. 5 represent the Landau-Fermi liquid (LFL) regime, where the in-plane quasiparticles are well defined, i.e., the magnitude of the scattering rate is smaller than energy $[1/\tau_{ab}(\omega) < \Omega]$. Data for $2H-NbSe_2$ falls in the LFL regime over the entire frequency interval in Fig. 5. However, this is not the case for the two cuprate materials. These differences in absolute values of the scattering rate may have a profound effect on the interplane transport. In $2H-NbSe_2$, where the in-plane quasiparticles are well defined, the interplane transport is also coherent, and is characterised by a narrow Drude-like mode, whose width decreases with temperature (Fig. 5c).

On the other hand, in $YBa_2Cu_3O_{6.6}$, which is lacking well-defined quasiparticles, the interplane transport is incoherent, with $\sigma_c(\omega)$ being dominated by optical phonons (Fig. 5a). As for the over-doped $YBa_2Cu_3O_7$ (Fig. 5b), the optical conductivity of this compound is between these two opposite limits. Fig. 5 therefore supports the notion that long-lived in-plane quasiparticles may be a necessary prerequisite for coherent out-of-plane transport.

One outcome of analysis of the energetic trends in the interlayer response is that the kinetic energy change is found exclusively in the materials for which the normal state properties are characterised by strong incoherence and are therefore distinct from the conventional Fermi-liquid picture. The hallmark of incoherent response in the spectra of $\sigma_{1c}(\omega)$ is a flat nearly featureless background (Fig. 2 and Fig. 5a, d). The kinetic energy is lowered upon the superconducting transition only if this characteristic behaviour is observed in the normal-state response. This is primarily the case in underdoped cuprates. As doping progresses to the optimal and over-doped regions of the phase diagram, the interlayer response becomes more coherent, as witnessed by the development of the Drude-like mode in $\sigma_{1c}(\omega)$. The magnitude of the kinetic energy change is reduced and eventually vanishes in the overdoped regime. Thus, it appears that the lowering of the kinetic energy characterises the transition to the coherent state at $T < T_c$, provided the coherence is lacking above the T_c. The formation of the pseudogap 'enhances' the non-Fermi liquid character.

In conclusion, a brief overview of the superconducting response in underdoped high-Tc superconductors reveals an interesting interplay between distinctive properties of a superconducting condensate in these systems and anomalies

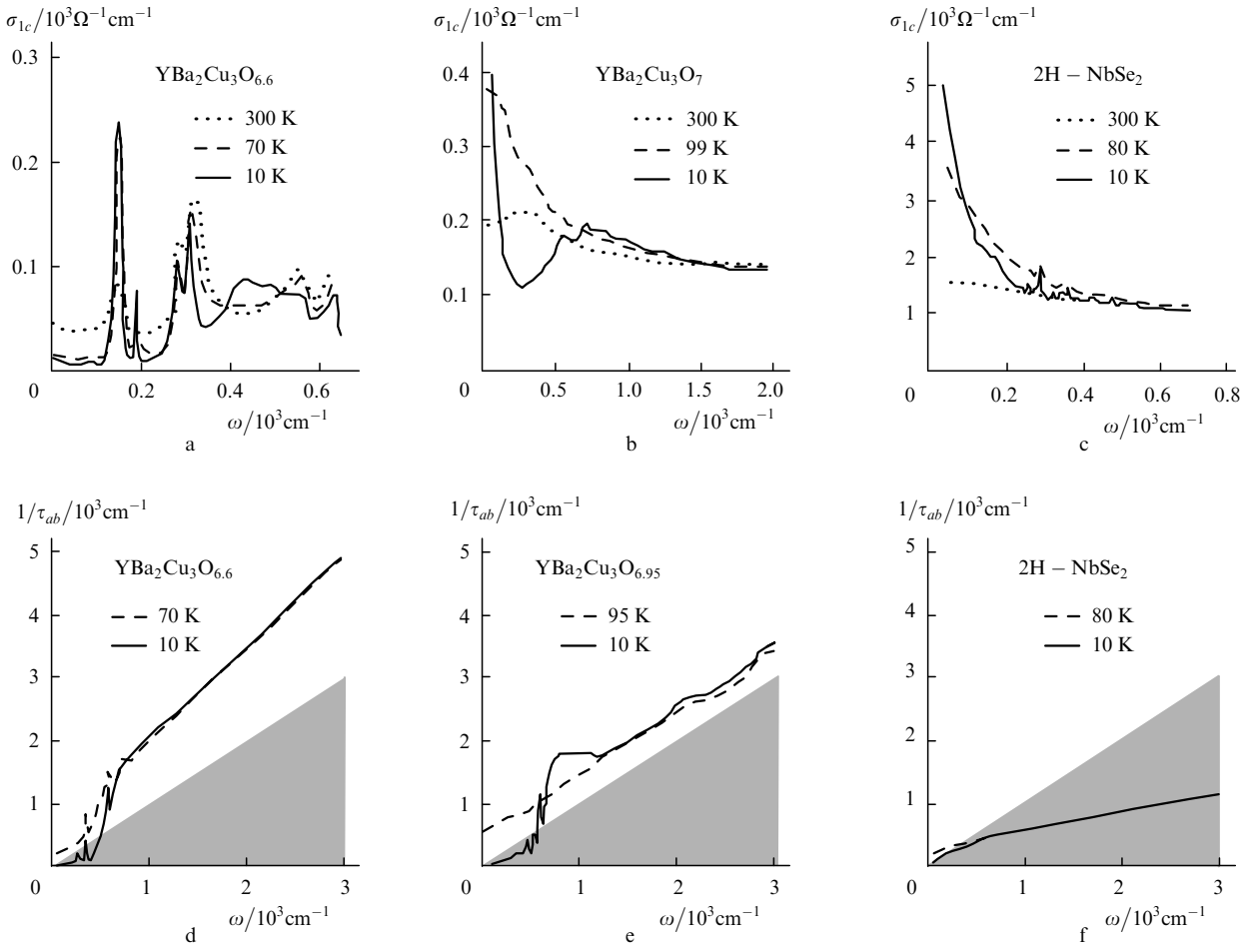

Figure 5. Examples of the interplane transport for layered superconductors [14]. Top panels show the real part of the out-of-plane optical conductivity $\sigma_{1c}(\omega)$; the bottom panels display the corresponding in-plane scattering rate $1/\tau_{ab}(\omega)$. The observation of the Drude-like feature in the interplane optical conductivity of the dichalcogenide $2H-NbSe_2$ (c) is consistent with magnetoresistance measurements, which revealed evidence for well-behaved quasiparticles. In contrast the conductivity of underdoped $YBa_2Cu_3O_{6.6}$ material (a) gives no signs of coherent response. Overdoped cuprates show the emergence of a Drude-like feature (b) and also occupy an intermediate position between the two lines in Fig. 3. Experimental data: $YBa_2Cu_3O_{6.6}$ [19, 18]; $YBa_2Cu_3O_7$ [20, 21]; $YBa_2Cu_3O_{6.95}$ [19]; $2H-NbSe_2$ [22].

of the normal state response. A giant energy scale involved into the formation of a superconducting condensate can be interpreted in terms of lowering of the electronic kinetic energy at $T < T_c$. This effect appears to be intimately connected with the lack of coherence in the normal-state response of underdoped cuprates.

Acknowledgements. I am grateful to Nikolai G. Basov for numerous discussions of issues addressed in this paper and beyond, which continued until his untimely death in July 2001. This work was supported by the NSF and DOE.

References

1. Basov D.N., Woods S.I., Katz A.S., Singley E.J., Dynes R.C., Xu M., Hinks D.G., Homes C.C., Strongin M. *Science*, **283**, 49 (1999).
2. Cooper S.L., Gray K.E., in *Physical Properties of High-T_c Superconductors*. Ed. by D.M. Ginsberg (Singapore: World Scientific, 1994) Vol. IV.
3. Hasegawa S., Ikuta H., Kitazawa K., in *Physical Properties of High-T_c Superconductors*. Ed. by D.M. Ginsberg (Singapore: World Scientific, 1992) Vol. 3, ch. 7.
4. Anderson P.W. *The Theory of Superconductivity in the High-T_c Cuprates* (Princeton: Princeton University Press, 1998); *Science*, **279**, 1196 (1998).
5. Chakravarty S. *Eur. Phys. J. B*, **5**, 337 (1998); Chakravarty S., Kee H.-Y., Abrahams E. *Phys. Rev. Lett.*, **82**, 2366 (1999).
6. Basov D.N., Timusk T., in *Handbook on the Physics and Chemistry of Rare Earths* (Amsterdam: Elsevier Science, 2001) Vol. 31, pp 437 – 507.
7. Timusk T., Statt B. *Rep. Prog. Phys.*, **62**, 61 (1999).
8. Homes C.C., Reedyk M.A., Crandels D.A., Timusk T. *Appl. Opt.*, **32**, 2976 (1993).
9. Basov D.N., Mook H.A., Dabrowski B., Timusk T. *Phys. Rev. B*, **52**, R13141 (1995).
10. Tamasaku K., Nakamura Y., Uchida S. *Phys. Rev. Lett.*, **69**, 1455 (1992).
11. Kim J.H., et al. *Physica C*, **247**, 297 (1995).
12. Uchida S., Tamasaku K., Tajima S. *Phys. Rev. B*, **53**, 1 (1996).
13. Basov D.N., Timusk T., Dabrowski B., Jorgensen J.D. *Phys. Rev. B*, **50**, 3511 (1994).
14. Dordevic S.V., Singley E.J., Basov D.N., Komiya S., Ando Y., Bucher E., Homes C.C., Strongin M. *Phys. Rev. B*, **65**, 134511 (2002).
15. Katz A.S., Woods S.I., Singley E.J., Li T.W., Xu M., Hinks D.G., Dynes R.C., Basov D.N. *Phys. Rev. B*, **61**, 5930 (2000).
16. Panagopoulos C., Cooper J.R., Xiang T., Wang Y.S., Chu C.W. *Phys. Rev. B*, **61**, 3808 (2000).

17. Hirsch J.E. *Physica C*, **199**, 305 (1992).
18. Homes C.C., Timusk T., Liang R., Bonn D.A., Hardy W.N. *Phys. Rev. Lett.*, **71**, 1645 (1993).
19. Basov D.N., Liang R., Dabrowski B., Bonn D.A., Hardy W.N., Timusk T. *Phys. Rev. Lett.*, **77**, 4090 (1996).
20. Schutzmann J., Tajima S., Miyamoto S., Tanaka S. *Phys. Rev. Lett.*, **73**, 174 (1994).
21. Tajima S., Schutzmann J., Miyamoto S., Terasaki I., Sato Y., Hauff R. *Phys. Rev. B*, **55**, 6051 (1997).
22. Dordevic S.V., Basov D.N., Dynes R.C., Bucher E. *Phys. Rev. B*, **64**, R161103 (2001).
23. Puchkov A.V., Fournier P., Basov D.N., Timusk T., Kapitulnik A., Kolesnikov N.N. *Phys. Rev. Lett.*, **77**, 3212 (1996).
24. Puchkov A.V., Basov D.N., Timusk T. *J. Phys. Cond. Mat.*, **8**, 10049 (1996).
25. Rotter L.D., Schlesinger Z., Collins R.T., Holtzberg F., Field C., Welp U.W., Crabtree G.W., Liu J.Z., Fang Y., Vandervoort K.G., Fleshler S. *Phys. Rev. Lett.*, **67**, 2741 (1991).

Nikolai Gennadievich Basov and his wife Kseniya Tikhonovna with their elder son Gennadii and yonger son Dmitrii.